

FE approach with Green's function as internal trial function for simulating bioheat transfer in the human eye

H. WANG^{1,2}, Q. H. QIN²

¹*Institute of Scientific and Engineering Computation
Henan University of Technology
Zhengzhou, China, 450052*

²*School of Engineering
Australian National University
Canberra ACT 0200, Australia
e-mail: qinghua.qin@anu.edu.au*

SIMULATION OF BIOHEAT TRANSFER in a human eye model is performed, using a newly developed Green's-function-based finite element formulation, named HFS-FEM. Non-linear radiation conditions are first treated by introducing an effective convection coefficient, and then two independent temperature fields are assumed within the element and along its boundary, respectively. Subsequently, a hybrid variational functional including the convection effect is constructed to guarantee the inter-element field continuity and to establish a linkage between the two independent fields. By virtue of the use of Green's functions as trial functions, the resulting nonlinear system contains only the element boundary integrals and is solved with an iteration technique. The results obtained are compared with those from ABAQUS and a good agreement is observed. Subsequently, the effect of control parameters is investigated to determine the temperature variation in the eye model; the results show that the proposed hybrid computational method is an effective tool for investigating the thermal performance of the human eye.

Key words: bioheat transfer, human eye, hybrid finite element approach, Green's function.

Copyright © 2010 by IPPT PAN

1. Introduction

Prediction of bioheat transport in a biological system is important in many diagnostic and therapeutic applications. However, biological tissues, such as the human eye consisting of several subdomains with different material properties, usually have complex geometry and thus its analytical prediction is difficult in practice. The application of computational methods in modeling biological systems is currently attracting increased attention with the rapid development of computer science.

Among the numerical methods developed so far, finite element and boundary element techniques have been widely used to analyze bioheat transfer phenomena in the human eye. For example, finite element formulations for two-dimensional human eye structures were developed by SCOTT [1], and NG *et al.* [2], who used the commercial software FEMLAB3.1 as a computing tool. By considering the natural circulation of aqueous humor, OOI *et al.* [3] utilized the finite element technique to conduct the heat transfer analysis for two-dimensional eye problems. A cylindrical eye model based on the finite element method was developed by BRINKMANN *et al.* [4]. For the finite element method (FEM), the solution domain is firstly divided into several cells or elements with independent material definitions, and in each subdomain, the physical fields are approximated by appropriate polynomial interpolations. A weak-form integral functional is developed to produce the final stiffness equations. However, the domain integrals and discontinuity of heat flux components between elements are disadvantages in the majority of conventional FEM. Additionally, refined meshes are necessary in FEM to achieve meaningful results for those regions near a local defect, such as holes, cracks, inclusions and so on. It should be also mentioned that the finite volume method (FVM) [5, 6] and the finite difference method (FDM) [7] have been employed to study transient temperature responses in the human eye caused by a laser source.

Besides the domain-type methods mentioned above, boundary element methods (BEM) or dual reciprocity BEM (DRBEM) involving boundary integrals only have also been applied to numerical thermal analysis in human eye structures [8–11]. Unlike FEM, FVM and FDM, the BEM formulation contains boundary integrals only. However, the treatment of singular or near-singular boundary integrals is usually quite tedious and inefficient and an extra boundary integral equation is also required to evaluate the interior fields inside the domain; additionally, for solving multi-domain problems with BEM, each region is dealt with separately and then the whole body is linked together by applying compatibility and equilibrium conditions along the interfaces between the subregions. As a result, the implementation of the BEM becomes quite complicated and the nonsymmetrical coefficient matrix of the resulting equations weakens the advantages of BEM. More discussion on FEM and BEM can be found in the literature [12, 13].

To alleviate some of these difficulties encountered in BEM and FEM, while retaining all of their advantages, a novel hybrid finite element model with Green's functions (also known as fundamental solutions), as a trial function, was recently developed by WANG and QIN [14–16] to deal with heat transfer problems and anisotropic elastic problems. In the new hybrid finite element model, two independent fields (one defined in the element domain and the other on the element boundary) are constructed, using Green's functions and conventional shape

functions used in BEM, respectively. A new hybrid variational functional is constructed to link these two independent fields for producing the final standard force-displacement equation system. Noting that the intra-element field approximated by the linear combination of Green's function analytically satisfies the related governing equation, the domain integrals in the hybrid functional can be directly converted into boundary integrals without any appreciable increase in computational effort. It is worth pointing out that no singular integrals are involved in the HFS-FEM, although the Green's function has been employed in the model. The reason is that the sources used for the evaluation of Green's function are placed outside the element of interest, as in the method of fundamental solution (MFS) [17–19]; thus, the source point and field point can never overlap during the computation. Moreover, the features of two independent interpolation fields and element boundary integral in HFS-FEM make the algorithm have potential applications in the aspect of mesh reduction by constructing specially-purposed elements such as functionally graded element, hole element, crack element, and so on.

In the present paper, the Green's-function-based FEM is extended to predict the steady-state temperature distribution of the eyeball in two-dimensional space with nonlinear boundary conditions. Linearization of the nonlinear radiation condition is first conducted by introducing the equivalent convection coefficient based on the iteration procedure, and then the modified hybrid variational functional is established to include the convection effect and produce the linkage between independent internal and boundary fields. The results obtained by means of the proposed algorithm are verified by comparison with those from ABAQUS[®]¹⁾, and different control parameters are investigated to reveal their bioheat effect.

2. Mathematical model of the human eye

A typical 2D model of the human eye sketched in Fig. 1 is considered here. It should be mentioned that only cornea, iris, lens, aqueous humor, sclera, vitreous and optic nerve are involved in the figure. In fact, between the sclera and the vitreous, there are two thin layers known as retina and choroid. Since these two layers are relatively thin, they are usually modeled together with the sclera and the optic nerve as a single homogeneous region [2]. Moreover, for the sake of simplicity, each of the subdomains is assumed to be thermally isotropic and homogeneous, and their conductivities are listed in Table 1, based on data in the literature [1, 2, 8, 9]. Table 1 also lists various thermal properties of the lens for different water contents caused by aging [2].

¹⁾ABAQUS 6.9, <http://www.simulia.com/>

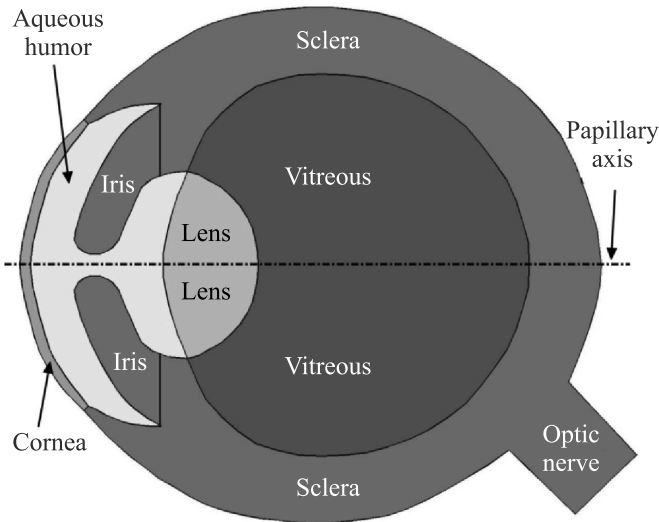


FIG. 1. Sketch diagram of the human eye.

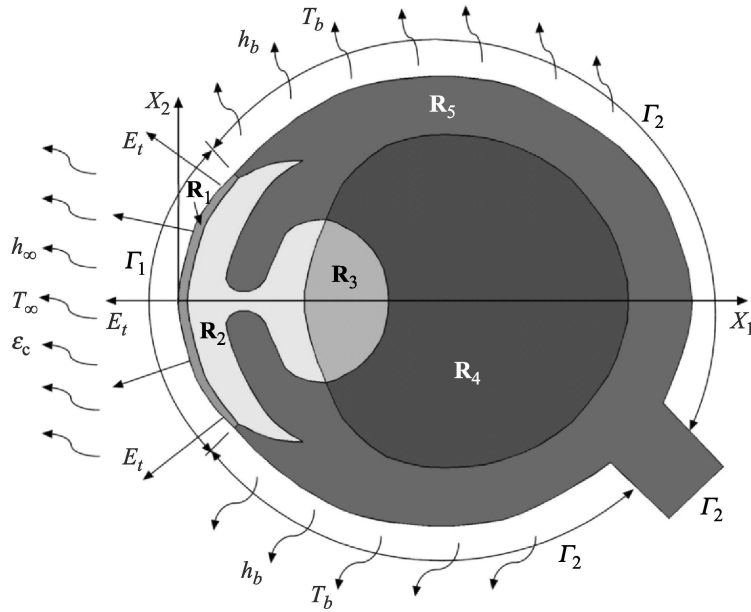


FIG. 2. The computational model and surface boundary conditions.

For convenience, the cornea and the aqueous humor are denoted by R_1 and R_2 , respectively, as shown in Fig. 2. The other two regions that are the lens and the vitreous are denoted by R_3 and R_4 , respectively. As it can be seen in Table 1, the iris and the sclera have the same thermal conductivity and are contiguous, so they can be modeled as a single homogeneous region, denoted by R_5 in the practical computation.

Table 1. Thermal conductivity of the subdomains in the human eye.

Subdomains	Thermal conductivity (W/mK)
Cornea	0.58
Aqueous humor	0.58
Sclera	1.0042
Iris	1.0042
Lens	0.21–0.54
Vitreous	0.603

In the analysis, a rectangular coordinate system (X_1, X_2) with the axis X_1 coinciding with the pupillary axis is employed. Under the coordinate system, the governing equation representing the bioheat transfer can be written by the well-known Pennes equation, addressing the effect of blood perfusion and metabolic activities in the biological system [20]:

$$(2.1) \quad k\nabla^2 T + \rho_b c_b w_b (T - T_b) + Q_m + Q_i = \rho c \frac{\partial T}{\partial t},$$

where

$$\nabla^2 = \frac{\partial^2}{\partial X_1^2} + \frac{\partial^2}{\partial X_2^2}$$

denotes the Laplace operator, t the time variable, ρ the density of the tissue, c the tissue specific heat, k the tissue thermal conductivity, w_b the blood flow rate, ρ_b the blood density, c_b the blood specified heat, T the unknown tissue temperature, T_b the blood temperature, Q_m the metabolic heat source term, and Q_i the internal heat source, which may be caused by external laser heating, electric disturbance or radiation of electromagnetic waves.

In this work, our interest is to determine the maximum temperature increase in the human eye, so we assume that a steady-state temperature is reached. Besides, in the human eye, only small parts of the eyeball, such as the sclera and optic nerve, are perfused and have metabolic activity (see Table 1 in [21]), so blood perfusion and metabolic heat generation can be disregarded [2, 8]. The resulting governing equation is reduced to a classic Laplace-type equation in the absence of external heat source. If the temperature in the region R_i is represented by T_i , then the heat flow Eq. (2.1) can be simplified to

$$(2.2) \quad k_i \nabla^2 T_i(\mathbf{x}) = 0, \quad \mathbf{x} \in R_i \quad (i = 1, 2, 3, 4, 5),$$

where k_i is the thermal conductivity of the region i , and no summation occurs in Eq. (2.2) and subsequent equations for the repeated subscript.

The following boundary conditions are added to the biological system:

- (1) Convection, radiation and tear evaporation on the corneal surface Γ_1 .

Since the cornea is the only region in the eye that is exposed to the environment, the heat loss caused through convection and radiation should be considered. Also, the evaporation of tears on the corneal surface increases the cooling rate on the corneal surface. Thus, three forms of cooling mechanism can be combined and the related boundary condition on the surface of cornea is written by [2, 3, 8, 21]

$$(2.3) \quad q_1 \equiv -k_1 \frac{\partial T_1}{\partial n} = h_\infty(T_1 - T_\infty) + \varepsilon_c \sigma(T_1^4 - T_\infty^4) + E_t \quad \text{on } \Gamma_1,$$

where n is the unit outward normal to the surface, h_∞ the heat transfer coefficient between the eye and ambient environment, T_∞ the sink temperature, σ the Stefan-Boltzman constant with value $5.669 \times 10^{-8} \text{ W/m}^2\text{K}^4$, ε_c the corneal emissivity, and E_t the heat loss due to tear evaporation.

(2) Convection condition on the outer surface Γ_2 of the sclera.

On the outer surface of the sclera, the heat flows run into the eye with the complicated network of ophthalmic vessels which are located inside the choroidal layer acting as a heating source to the sclera. To simulate this heating mechanism, the human eye is assumed to be embedded in a homogeneous surrounding anatomy such that the heat exchange between the eye and the surrounding may be modeled using the following convection boundary condition [2, 3, 8, 21]:

$$(2.4) \quad q_2 \equiv -k_2 \frac{\partial T_2}{\partial n} = h_b(T_2 - T_b) \quad \text{on } \Gamma_2,$$

where h_b denotes the blood convection coefficient from the sclera to the body core, and T_b is the temperature of the surrounding blood.

(3) Continuous conditions on the interfaces between any two contiguous regions R_i and R_j in the eye

$$(2.5) \quad T_i = T_j, \quad q_i + q_j = 0 \quad \text{on } R_i \cap R_j.$$

3. Hybrid finite element approach

3.1. Treatment of nonlinear radiation condition

The presence of the nonlinear radiation term in the boundary conditions makes the problem difficult to formulate. This difficulty can be resolved by introducing a suitable iterative procedure. For this purpose, we recast the nonlinear boundary condition (2.3) as

$$(3.1) \quad q_1 \equiv -k_1 \frac{\partial T_1}{\partial n} = [h_\infty + \varepsilon \sigma(T_1 + T_\infty)(T_1^2 + T_\infty^2)] (T_1 - T_\infty) + E_t$$

from which we can see that if the term $(T_1 + T_\infty)(T_1^2 + T_\infty^2)$ is known, the condition (3.1) can be viewed as a generalized convection condition. Based on this concept, we design the following iterative algorithm:

$$(3.2) \quad q_1 \equiv -k_1 \frac{\partial T_1^{(m)}}{\partial n} = h(T_1^{(m)} - T_\infty) + E_t$$

with

$$(3.3) \quad h = h_\infty + \varepsilon \sigma (T_1^{(m-1)} + T_\infty) [(T_1^{(m-1)})^2 + T_\infty^2],$$

where $\{T_1^{(m)}\}$ are temperature sequences for $m = 1, 2, 3, \dots$, and $T_1^{(0)}$ represents an initial guess as to temperature.

The iteration is completed when the convergent condition related to the inter-iteration difference is satisfied:

$$(3.4) \quad \|T_1^{(m)} - T_1^{(m-1)}\|_\infty \leq \delta,$$

where δ is a sufficiently small real number representing a specified iteration tolerance; for example, $\delta = 10^{-6} \text{ }^\circ\text{C}$ can be used in the subsequent calculation.

3.2. Hybrid finite element formulation

The temperature and heat flux in any iteration step can be evaluated by the Green's-function-based finite element model. For the sake of simplicity, the subscripts attached to temperature, heat flux and thermal conductivity representing the region number and the superscript representing iteration step, are discarded. In this model, the temperature in a particular element e occupying the domain Ω_e with boundary Γ_e is approximated by the linear combination of Green's functions, as it was done in the method of fundamental solution (MFS) [17–19],

$$(3.5) \quad T(P) = \sum_{j=1}^{n_s} T^*(P, Q_j) c_{ej} = \{\mathbf{N}\} \{\mathbf{c}_e\}.$$

Differentiation of Eq. (3.5) with respect to the outward normal gives

$$(3.6) \quad q \equiv -k \frac{\partial T}{\partial n} = \begin{Bmatrix} n_1 & n_2 \end{Bmatrix} \begin{Bmatrix} -k \frac{\partial T}{\partial X_1} \\ -k \frac{\partial T}{\partial X_2} \end{Bmatrix} \\ = \begin{Bmatrix} n_1 & n_2 \end{Bmatrix} \begin{Bmatrix} -k \frac{\partial \{\mathbf{N}\}}{\partial X_1} \\ -k \frac{\partial \{\mathbf{N}\}}{\partial X_2} \end{Bmatrix} \{\mathbf{c}_e\} = \{\mathbf{Q}\} \{\mathbf{c}_e\},$$

where P is a field point which may be located within the element or on its boundary, Q_j is a source point placed outside the element to avoid the singularity of the Green's function with unknown source intensity c_j , $T^*(P, Q_j)$ is the temperature response at the point P due to the unit point heat source applied at the point Q_j

$$(3.7) \quad T^*(P, Q_j) = -\frac{1}{2\pi k} \ln \|P - Q_j\|.$$

In Eq. (3.5), it is important to determine the position of source point Q_j . Following the way in our previous work [14–16], the location of sources Q_j ($j = 1, 2, \dots, n_s$) is determined by a non-dimensionless parameter $\gamma = (Q_j - P_b)/P_b > 0$, which represents a distance between the element boundary point P_b and the sources, and which may be chosen in a wide range ($2 \leq \gamma \leq 9$ in our analysis) to give stable and accurate results [14–16].

Meanwhile, an independent frame field defined over the element boundary is assumed in the form

$$(3.8) \quad \tilde{T}_e(P) = \sum_{i=1}^{n_d} \tilde{N}_i d_i = \{\tilde{\mathbf{N}}\} \{\mathbf{d}_e\},$$

where \tilde{N}_i stands for the conventional 1D shape functions as used in BEM, and d_i is the unknown nodal temperature.

To establish the linkage between the two independent fields (3.5) and (3.8) and to include the effective convection boundary condition (3.2), a modified hybrid variational functional is constructed based on the authors' previous work [14]:

$$(3.9) \quad \begin{aligned} \Pi_{me} = & -\frac{1}{2} \int_{\Omega_e} k \left[\left(\frac{\partial T}{\partial X_1} \right)^2 + \left(\frac{\partial T}{\partial X_2} \right)^2 \right] d\Omega \\ & - \int_{\Gamma_{qe}} \bar{q} \tilde{T} d\Gamma + \int_{\Gamma_e} q (\tilde{T} - T) d\Gamma - \frac{1}{2} \int_{\Gamma_{ce}} h (\tilde{T} - T_\infty)^2 d\Gamma, \end{aligned}$$

in which the last boundary integral reflects the effective convection effect, Γ_{qe} and Γ_{ce} respectively denote the heat flux and convective boundaries, and \bar{q} represents the specified boundary heat flux.

By invoking the divergence theorem

$$(3.10) \quad \int_{\Omega} \left(\frac{\partial f}{\partial X_1} \frac{\partial h}{\partial X_1} + \frac{\partial f}{\partial X_2} \frac{\partial h}{\partial X_2} \right) d\Omega = \int_{\Gamma} h \frac{\partial f}{\partial n} d\Gamma - \int_{\Omega} h \nabla^2 f d\Omega$$

for any continuous functions f and h in the domain, the first-order variational can be expressed as

$$(3.11) \quad \delta \Pi_{me} = \int_{\Omega_e} k \nabla^2 T \delta T d\Omega - \int_{\Gamma_{qe}} (\bar{q} - q) \delta \tilde{T} d\Gamma + \int_{\Gamma_{Ie}} q \delta \tilde{T} d\Gamma \\ + \int_{\Gamma_e} (\tilde{T} - T) \delta q d\Gamma - \int_{\Gamma_{ce}} h (\tilde{T} - T_\infty) \delta \tilde{T} d\Gamma,$$

in which the first and second integrals enforce the governing equation and the heat flux boundary conditions, the third and fourth integrals enforce the inter-element continuity condition, and the last integral enforces the convection boundary condition.

Since the internal field T defined in Eq. (3.5) satisfies analytically the governing equation (2.2), the domain integral in Eq. (3.9) can be straightforwardly converted into a boundary integral defined on the element boundary, and we finally have

$$(3.12) \quad \Pi_{me} = -\frac{1}{2} \int_{\Gamma_e} q T d\Gamma - \int_{\Gamma_{qe}} \bar{q} \tilde{T} d\Gamma + \int_{\Gamma_e} q \tilde{T} d\Gamma - \int_{\Gamma_{ce}} \frac{h}{2} (\tilde{T} - T_\infty)^2 d\Gamma.$$

Substituting Eqs. (3.5) and (3.8) into Eq. (3.12) yields

$$(3.13) \quad \Pi_{me} = -\frac{1}{2} \{\mathbf{c}_e\}^T [\mathbf{H}_e] \{\mathbf{c}_e\} - \{\mathbf{d}_e\}^T \{\mathbf{g}_e\} + \{\mathbf{c}_e\}^T [\mathbf{G}_e] \{\mathbf{d}_e\} \\ - \frac{1}{2} \{\mathbf{d}_e\}^T [\mathbf{F}_e] \{\mathbf{d}_e\} + \{\mathbf{d}_e\}^T \{\mathbf{f}_e\} - \{\mathbf{a}_e\}.$$

By virtue of the stationary condition

$$(3.14) \quad \frac{\partial \Pi_{me}}{\partial \{\mathbf{c}_e\}^T} = \{\mathbf{0}\}, \quad \frac{\partial \Pi_{me}}{\partial \{\mathbf{d}_e\}^T} = \{\mathbf{0}\},$$

we have the following stiffness equations for determining all unknowns:

$$(3.15) \quad [\mathbf{K}_e] \{\mathbf{d}_e\} = \{\mathbf{g}_e\} - \{\mathbf{f}_e\}, \quad \{\mathbf{c}_e\} = [\mathbf{H}_e]^{-1} [\mathbf{G}_e] \{\mathbf{d}_e\},$$

where

$$(3.16) \quad [\mathbf{H}_e] = \int_{\Gamma_e} \{\mathbf{Q}\}^T \{\mathbf{N}\} d\Gamma, \quad [\mathbf{G}_e] = \int_{\Gamma_e} \{\mathbf{Q}\}^T \{\tilde{\mathbf{N}}\} d\Gamma \\ [\mathbf{F}_e] = \int_{\Gamma_{ce}} h \{\tilde{\mathbf{N}}\}^T \{\tilde{\mathbf{N}}\} d\Gamma, \quad \{\mathbf{f}_e\} = \int_{\Gamma_{ce}} h T_\infty \{\tilde{\mathbf{N}}\}^T d\Gamma, \\ \{\mathbf{g}_e\} = \int_{\Gamma_{eq}} \{\tilde{\mathbf{N}}\}_e^T \bar{q} d\Gamma, \quad \{\mathbf{a}_e\} = \int_{\Gamma_{ce}} \frac{h T_\infty^2}{2} d\Gamma.$$

4. Numerical results

To simulate the temperature distribution and investigate the effect of control parameters on the temperature variation in the eye model, the approach presented here is applied to a practical example, and the results obtained are compared with those from ABAQUS. For reference, the values of the control parameters related to the outer boundary conditions are listed in Table 2 [1, 2]. It should be mentioned that the geometrical dimensions of the computing model employed in this paper are taken from the literature [8] and regenerated; therefore, the geometrical dimensions of the computing model here might differ from those in [8] and the results may thus show some discrepancy with those from [8].

Table 2. Control parameters associated with boundary conditions.

Control parameters	Value
Blood temperature T_b	37 ($^{\circ}\text{C}$)
Blood convection coefficient h_b	65 ($\text{Wm}^{-2}\text{K}^{-1}$)
Ambient temperature T_{∞}	10–40 ($^{\circ}\text{C}$)
Ambient convection coefficient h_{∞}	8–100 ($\text{Wm}^{-2}\text{K}^{-1}$)
Cornea surface emissivity ε_c	0.975
Evaporation rate of tear	20–320 (Wm^{-2})

4.1. Verification of the presented approach

The computational model is discretized with 1374 eight-node elements, and in total 4243 nodal degrees of freedom are included (see Fig. 3). For simplicity,

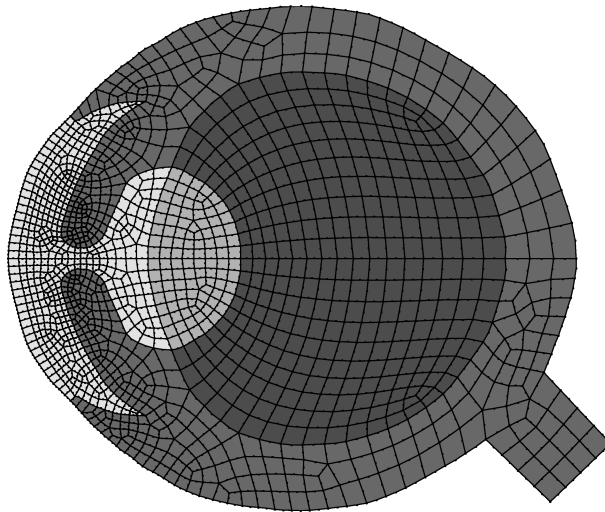


FIG. 3. Hybrid finite elements for human eye model.

in Tables 1 and 2, the thermal conductivity of lens is taken to be $0.4 \text{ Wm}^{-1}\text{K}^{-1}$, $T_\infty = 25^\circ\text{C}$, $h_\infty = 10 \text{ Wm}^{-2}\text{K}^{-1}$, and $E_t = 40 \text{ Wm}^{-2}$ here [8]. The initial guess for the temperature is taken to be the ambient temperature in the following calculation.

Firstly, the influence of the parameter γ is investigated and convergent results of temperature at the origin of coordinate system are shown in Fig. 4 with three iterations. It can be seen that there is a large range of the parameter γ which yields stable results ($2 \leq \gamma \leq 9$ from Fig. 4), and the unstable results are observed for the value of γ is less than 1 due to the near singular property of Green's function. The same conclusion can also be found in our previous work [14–16], so in the following computation, $\gamma = 5$ is employed.

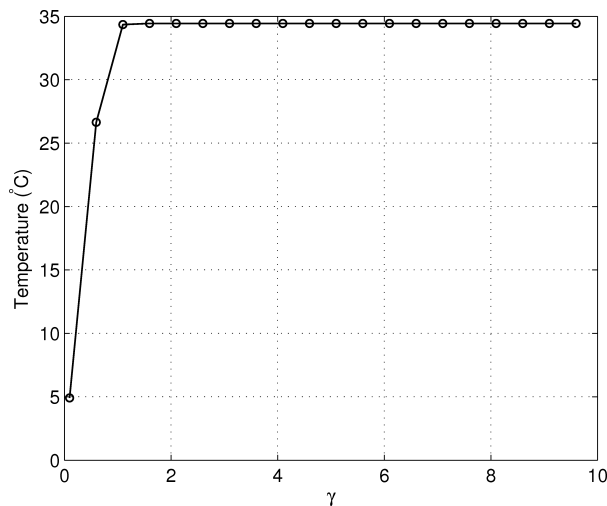


FIG. 4. Temperature variation at the origin of coordinate system with different γ .

Subsequently, the distribution of temperature along the papillary axis is plotted in Fig. 5, in which the results from ABAQUS with the same element mesh are provided for the purpose of comparison. It can be seen that good agreement is achieved between the proposed Green's-function-based FEM and ABAQUS. The temperature discrepancy between the two methods is only 0.001°C or percentage 0.004% at the center of the corneal surface. The temperature isotherms in the entire domain are displayed in Fig. 6, in which the solid lines represent the results of the proposed Green's-function-based FEM, and the dashed lines represent those from ABAQUS. As expected, good agreement is achieved between the results of HFS-FEM and those from ABAQUS. The presented computing model is therefore verified.

It should be noted that the radiation effect is smaller than the convection effect in practice, especially for the larger convection coefficient. This can be seen

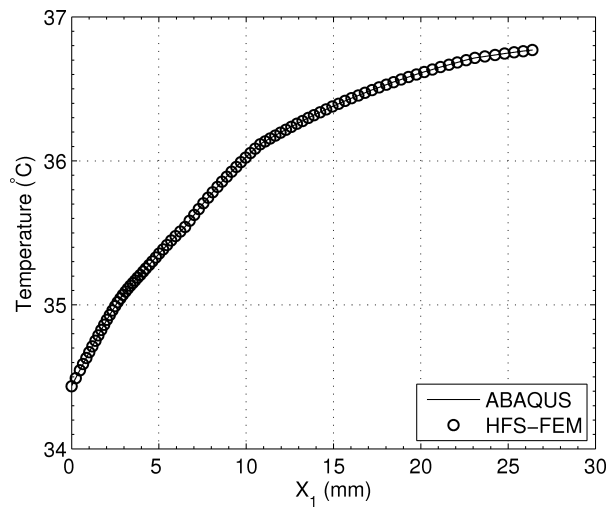


FIG. 5. Temperature distribution on the papillary axis.

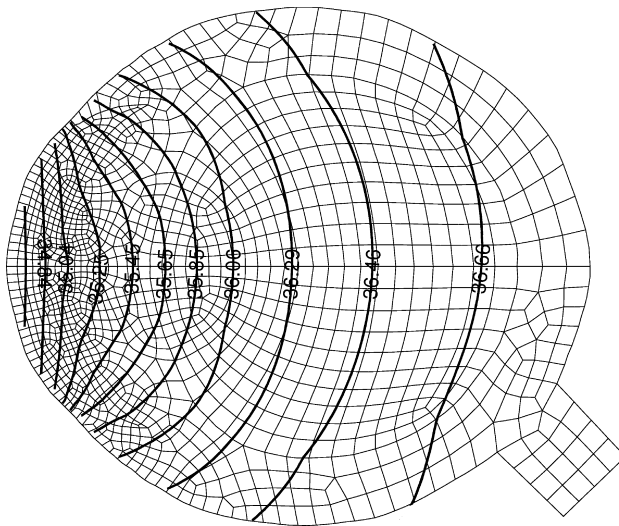


FIG. 6. Isothermal lines in the human eye domain.

from Eq. (3.3), in which h_∞ is usually much larger than

$$\varepsilon\sigma \left(T_1^{(m-1)} + T_\infty \right) \left[\left(T_1^{(m-1)} \right)^2 + T_\infty^2 \right].$$

In order to clearly show how the nonlinear iterative procedure works, the linear convection effect and tear evaporation effect on the corneal surface are discarded, that is, $h_\infty = 0$, $E_t = 0$. At the same time, to enlarge the radiation effect, the ambient temperature T_∞ is changed to 250°C . After 7 iterations, the convergent

temperature at the origin of coordinate system is achieved as 41.058°C , which agrees well with the result 41.062°C of ABAQUS. Thus, the constructed iteration procedure can be used to effectively deal with radiation problems.

4.2. Effect of tear evaporation

There is usually a thin lipid layer covering the corneal surface, the function of which is to prevent evaporation of tears from the corneal surface. When the layer is destroyed, the evaporation rate increases dramatically, and can reach as high as 320 Wm^{-2} , whereas the evaporation rate of normal eyes is in the range of $20\text{--}100\text{ Wm}^{-2}$ [2]. It is therefore necessary to investigate the effect of evaporation on temperature distribution in the eye model. In the following analysis, the temperature and convection coefficient of ambient fluid are taken to be 25°C and $10\text{ Wm}^{-2}\text{K}^{-1}$, respectively, and the thermal conductivity of the lens region is assumed to be $0.4\text{ Wm}^{-1}\text{K}^{-1}$. The temperature variation along the X_1 axis is shown in Fig. 7, from which the evaporation rate seems to be important in changing the corneal surface temperature. It is observed that either in the normal eye with evaporation rate in the range $[20\text{--}100]\text{ Wm}^{-2}$, or when the lipid layer is destroyed, there is an approximately steady decrease in the value of 0.16° at the center of the corneal surface for every increment in the value of 10 Wm^{-2} for evaporation rate, while a small change in temperature occurs at the rear of the eye, as expected. The detailed computing data is listed in Table 3. It is reasonable that the cooling effect increases as the evaporation rate increases. Additionally, good agreement is observed with the results obtained from ABAQUS with same mesh, and the accuracy of the proposed HFS-FEM is again verified.

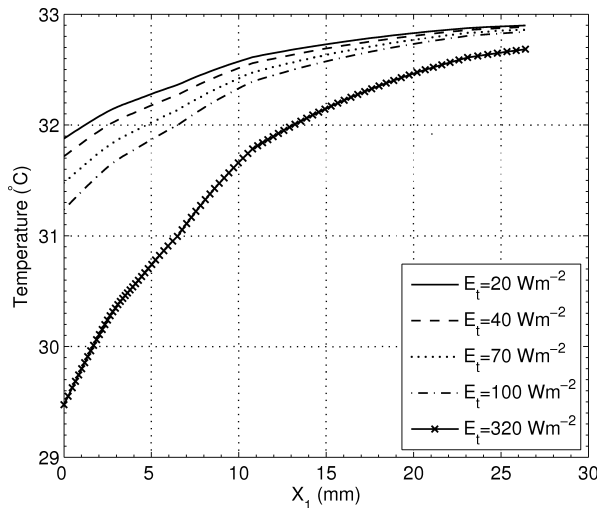


FIG. 7. Temperature variation on the papillary axis for different evaporation rates.

Table 3. Effects of evaporation rate on the temperature variation at the center of the cornea surface.

Evaporation rate E_t (Wm^{-2})	Temperature at the center of cornea surface ($^{\circ}\text{C}$)	
	HFS-FEM	ABAQUS
20	34.755	34.757
40	34.435	34.436
70	33.954	33.956
100	33.474	33.475
320	29.948	29.950

4.3. Effect of ambient fluid

The effect of ambient fluid can be analyzed by changing two parameters: ambient temperature T_{∞} and ambient convection coefficient h_{∞} . Here, values of T_{∞} in the range $[20-50]^{\circ}\text{C}$ and of h_{∞} in the range $[8-100] \text{Wm}^{-2}\text{K}^{-1}$ are considered to study the temperature response caused by these two parameters. The evaporation rate and the thermal conductivity of the lens are assumed to be 40Wm^{-2} and $0.4 \text{Wm}^{-1}\text{K}^{-1}$, respectively. The numerical results are presented in Figs. 8 and 9. It can be seen from Fig. 8 that an increase in the

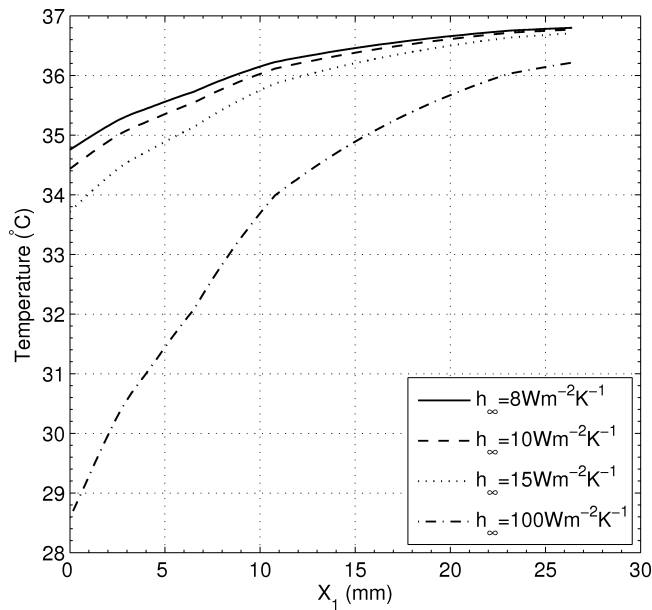


FIG. 8. Temperature variation on the papillary axis for different ambient convection coefficients ($T_{\infty} = 25^{\circ}\text{C}$).

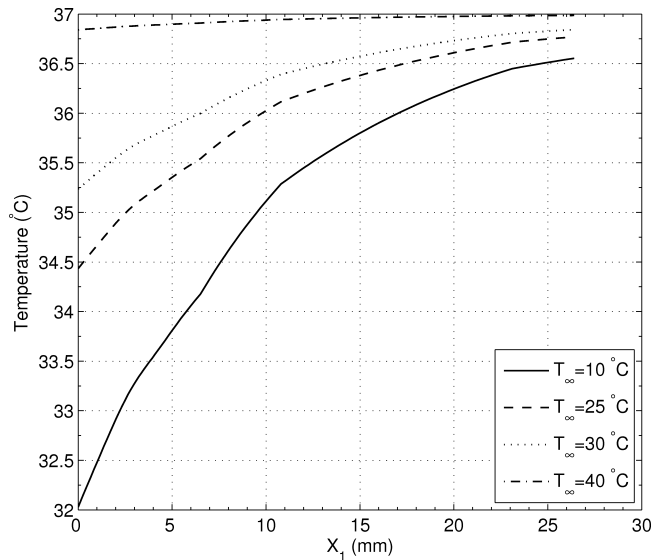


FIG. 9. Temperature variation on the papillary axis for different ambient convection coefficients ($h_{\infty} = 10 \text{ Wm}^{-2}\text{K}^{-1}$).

convection coefficient of ambient fluid inevitably brings more heat loss from the cornea surface, which finally leads to a low surface temperature. Meanwhile, it seems from Fig. 9 that the ambient temperature has a significant effect on the temperature at the center of the corneal surface. The lower is the ambient temperature, the greater will be the temperature difference between the cornea surface and the surrounding fluid. As a result, more heat energy is lost in the eye model.

4.4. Effect of lens thermal conductivity

Finally, the effect of thermal conductivity in the transparent lens region on the temperature distribution is studied. It is well known that the water content of the lens decreases as a result of aging and thus the lens becomes harder, causing different thermal conductivity [2]. For the purpose of comparison, the values of thermal conductivity of the lens are assumed to be in the range $[0.21\text{--}0.54] \text{ Wm}^{-1}\text{K}^{-1}$ [2]. Other control parameters, including ambient temperature, ambient convection coefficient, and evaporation rate, are assumed to be 25°C , $10 \text{ Wm}^{-2}\text{K}^{-1}$, and 40 Wm^{-2} , respectively. From the variation of temperature on the pupillary axis shown in Fig. 10 it is seen that very minor change occurs at the rear of the eye, while a temperature rise of 0.088°C is detected at the center of the cornea surface, due to the increase in the thermal conductivity of the lens. It is reasonable that higher values of thermal conductivity of the lens will permit more heat transfer from the rear of the eye (high

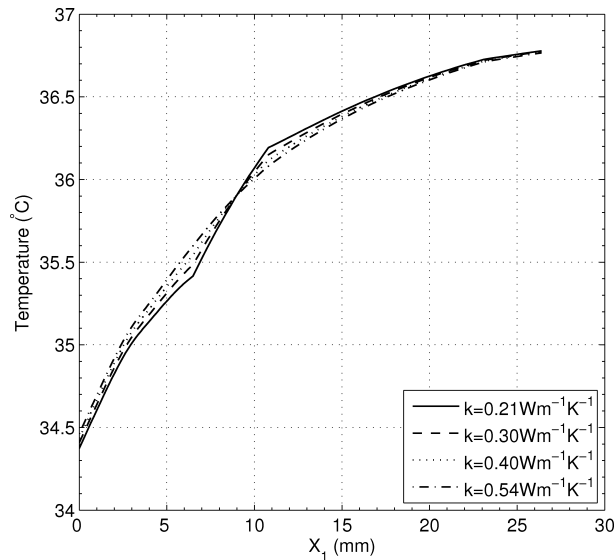


FIG. 10. Temperature variation on the papillary axis for different lens thermal conductivity.

temperature region) to the corneal surface (low temperature region), and thus cause the surface temperature to increase, although the influence is relatively small.

5. Conclusions

A hybrid finite element model with Green's function as the intra-element trial function for heat transfer analysis of the human eye, was developed to calculate the steady-state temperature distribution in a normal human eye. In the proposed formulation, by virtue of the use of Green's functions, the constructed variational functional involving the convection effect includes element boundary integrals only. Results of the presented algorithm were compared with those of ABAQUS, and their agreement shows promise for future applications in the human eye. Further, to understand and access thermal mechanisms in the eye model, a sensitivity analysis was performed by adjusting the values of specified control parameters, which are usually uncertain in practice. Numerical results showed that perturbations of evaporation rates significantly change the cooling effect on the temperature distribution in the anterior regions. The temperature distribution was also observed to be sensitive to variations of the ambient temperature and the ambient convection coefficient. Finally, it was found that variations in the thermal conductivity of the lens lead to minor changes in temperature in the anterior regions and negligible change at the rear of the eye.

References

1. J.A. SCOTT, *A finite element model of heat transport in the human eye*, Phys. Med. Biol., **33**, 227–242, 1988.
2. E.Y.K. NG, E.H. OOI, *FEM simulation of the eye structure with bioheat analysis*, Comput. Methods Programs Biomed., **82**, 268–276, 2006.
3. E.H. OOI, E.Y.K. NG, *Simulation of aqueous humor hydrodynamics in human eye heat transfer*, Comput. Biol. Med., **38**, 252–262, 2008.
4. R. BRINKMANN, N. KOOP, G. DROEGE, U. GROTEHUSMANN, A. HUBER, R. BIRNGRUBER, *Investigations on laser thermokeratoplasty*, [in:] Proceedings of the SPIE, Vol. 2079, pp. 120–130, Budapest, Hungary, 1994.
5. A. NARASIMHAN, K.K. JHA, L. GOPAL, *Transient simulations of heat transfer in human eye undergoing laser surgery*, Int. J. Heat Mass Transfer, **53**, 482–490, 2010.
6. K.J. CHUA, J.C. HO, S.K. CHOU, M.R. ISLAM, *On the study of the temperature distribution within a human eye subjected to a laser source*, Int. Commun. Heat Mass Transfer, **32**, 1057–1065, 2005.
7. M.A. MAINSTER, T.J. WHITE, J.H. TIPS, *Corneal thermal response to the CO₂ laser*, Appl. Opt., **9**, 665–667, 1990.
8. E.H. OOI, W.T. ANG, E.Y.K. NG, *Bioheat transfer in the human eye: A boundary element approach*, Eng. Anal. Bound. Elem., **31**, 494–500, 2007.
9. E.H. OOI, W.T. ANG, E.Y.K. NG, *A boundary element model of the human eye undergoing laser thermokeratoplasty*, Comput. Biol. Med., **38**, 727–737, 2008.
10. E.H. OOI, W.T. ANG, E.Y.K. NG, *A boundary element model for investigating the effects of eye tumor on the temperature distribution inside the human eye*, Comput. Biol. Med., **39**, 667–677, 2009.
11. A. PERATTA, *3D low frequency electromagnetic modelling of the human eye with boundary elements: Application to conductive keratoplasty*, Eng. Anal. Bound. Elem., **32**, 726–735, 2008.
12. Q.H. QIN, *The Trefftz finite and boundary element method*, WITpress, Southampton 2000.
13. Q.H. QIN, H. WANG, *Matlab and C programming for Trefftz finite element methods*, CRC Press, New York 2008.
14. H. WANG, Q.H. QIN, *Hybrid FEM with fundamental solutions as trial functions for heat conduction simulation*, Acta Mech. Solida Sin., **22**, 487–498, 2009.
15. H. WANG, L.L. CAO, Q.H. QIN, *Hybrid Graded Element Model for Nonlinear Functionally Graded Materials*, Mech. Adv. Mater Struct., accepted for publication.
16. H. WANG, Q.H. QIN, *Fundamental-solution-based finite element model for plane orthotropic elastic bodies*, Eur. J. Mech. A-Solid, **29**, 801–809, 2010.
17. H. WANG, Q.H. QIN, Y.L. KANG, *A new meshless method for steady-state heat conduction problems in anisotropic and inhomogeneous media*, Arch. Appl. Mech., **74**, 563–579, 2005.
18. H. WANG, Q.H. QIN, *A meshless method for generalized linear or nonlinear Poisson-type problems*, Eng. Anal. Bound. Elem., **30**, 515–521, 2006.

19. H. WANG, Q.H. QIN, Y.L. KANG, *A meshless model for transient heat conduction in functionally graded materials*, *Comput. Mech.*, **38**, 51–60, 2006.
20. H.H. PENNES, *Analysis of tissue and arterial blood temperatures in the resting human forearm*, *J. Appl. Physiol.*, **1**, 93–102, 1948.
21. V.M.M. FLYCKT, B.W. RAAYMAKERS, J.J.W. LAGENDIJK, *Modelling the impact of blood flow on the temperature distribution in the human eye and the orbit: fixed heat transfer coefficients versus the Pennes bioheat model versus discrete blood vessels*, *Phys. Med. Biol.*, **51**, 5007–5021, 2006.

Received July 5, 2010; revised version September 19, 2010.
